

# Model for doping-induced contrast in photoelectron emission microscopy

V. W. Ballarotto,<sup>a)</sup> K. Siegrist, R. J. Phaneuf, and E. D. Williams

Laboratory for Physical Sciences and Department of Physics, University of Maryland, College Park, Maryland 20740

(Received 17 July 2001; accepted for publication 3 October 2001)

We present a model that describes doping-induced contrast in photoelectron emission microscopy by including the effect of surface state distributions and doping-induced band gap reduction. To quantify the contrast, the photoyield from the valence band for near-threshold photoemission is calculated as a function of  $p$ -type doping concentration in Si(001). Various surface state distributions appropriate for a native-oxide covered Si device are investigated in order to determine the effect on doping-induced contrast. The lower limit on the number of surface states necessary for doping-induced contrast to occur is approximately  $5 \times 10^{13} \text{ cm}^{-3}$ . An interesting result is that neither the position nor the energy distribution of the surface donor states affects the contrast, which corresponds to approximately a factor of 2 change in intensity for each decade change in doping density. However, the overall intensity increases with any one of: increased surface state density, narrowing of surface state distribution, or increased energy of surface states with respect to the valence band. The band bending profile generated by the model predicts that doping-induced contrast will be affected by varying the incident photon energy. Experimentally, we verify this prediction by imaging with photon energies between 4.5 and 5.2 eV. © 2002 American Institute of Physics. [DOI: 10.1063/1.1423399]

## INTRODUCTION

To gain an understanding of photoelectron emission microscopy (PEEM) contrast relevant for semiconductor devices, we have quantitatively studied a simple device that produces only one type of contrast, namely, doping-induced contrast.<sup>1,2</sup> Figure 1 is a PEEM image of a  $p$ - $n$  junction array that makes up the device. This is a straightforward illustration of doping-induced contrast in silicon. The vertical B-doped lines have a concentration of  $10^{18} \text{ cm}^{-3}$  and the horizontal B-doped lines are  $3 \times 10^{19} \text{ cm}^{-3}$ . Clearly, the  $3 \times 10^{19} \text{ cm}^{-3}$  lines are brighter than the  $10^{18} \text{ cm}^{-3}$  lines, creating contrast with respect to each other as well as with the  $n$ -type substrate. Interpretation of the observed contrast requires a model that takes into account the effect of doping on the photothreshold of silicon.<sup>3,4</sup>

In our previous work, we used a model based on band bending principles to describe the photothreshold dependence on doping.<sup>1,2</sup> The model predicts that the magnitude of upward band bending in silicon increases as the boron concentration increases. As a result, the contrast observed in PEEM images of Si  $pn$  devices can be modeled reasonably well. However, the model is incomplete in that it does not include a realistic distribution of surface states nor does it adequately address degenerate doping. Therefore, it is necessary to develop a more physical model of doping-induced contrast.

We present here a general model that is an extension of the one we suggested previously. In addition to a more accurate calculation for a degenerately doped semiconductor, the

surface state distribution can be chosen to represent the condition of the sample. We investigate how different surface state distributions for a native-oxide covered silicon device affect doping-induced contrast in PEEM. The effect of varying the incident photon energy on the predicted doping-induced behavior is also examined experimentally with a tunable light source.

## EXPERIMENT

Imaging was done with spontaneous coherent radiation from the Duke University UV free electron laser (FEL). Data at the FEL was obtained using photon energies ranging from 4.5 to 5.2 eV with a focused intensity of  $10 \text{ W/cm}^2$ . The output spectrum of the FEL is nearly Gaussian with a full width at half maximum of approximately 0.13 eV.<sup>5</sup> The background pressure during imaging is roughly  $5 \times 10^{-10}$  Torr.

The samples used consisted of a lightly  $n$ -doped Si substrate ( $P$ ,  $10^{14} \text{ cm}^{-3}$ ), patterned and ion implanted to create regions of different  $p$  doping ( $B$ ,  $10^{17}$ – $10^{20} \text{ cm}^{-3}$  in the near surface region). The sample fabrication techniques have been described previously.<sup>2,6</sup>

Data were acquired using a commercial PEEM instrument.<sup>1,5</sup> A chevron-type multichannel plate is used to intensify the images roughly 1 000 000 times. A 12-bit charge-coupled device camera is used to record images that can be stored in either 16-bit tif or 8-bit bmp file formats. To make quantitative assessment of the PEEM intensity from each set of doping levels, sets of parallel line scans were measured from the image data. Typically, enough lines were averaged to produce an intensity profile with a rms fluctuation that is less than 1% of the average intensity from the  $n$ -type region.

<sup>a)</sup> Author to whom correspondence should be addressed; electronic mail: vince@lps.umd.edu

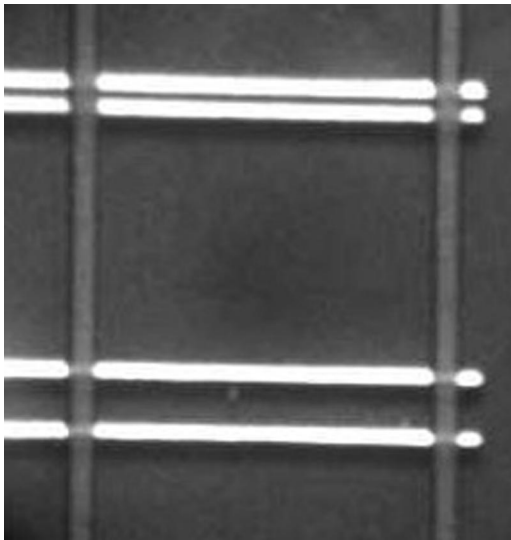


FIG. 1. PEEM image of lateral array of *pn* junctions illustrating doping-induced contrast in Si(001). The vertical lines are  $10^{18} \text{ cm}^{-3}$  B doped. The horizontal lines are  $3 \times 10^{19} \text{ cm}^{-3}$  B doped. The field of view is  $\approx 40 \mu\text{m}$ .

## THEORY

In order to model doping-induced contrast, it is necessary to understand the variation in photoyield as a function of doping concentration. To accomplish this, we consider near-threshold photoemission. For indirect, near-threshold optical transitions, the photoyield  $Y$  from the valence band<sup>7</sup> can be expressed as

$$Y(h\nu, N) = C_N \int (h\nu - E_T(x, N))^{5/2} e^{-x/l} dx, \quad (1)$$

where  $h\nu$  is the photon energy and  $E_T(x, N)$  is the photothreshold as a function of depth  $x$  and doping concentration  $N$ . The constant  $C_N$  depends on the incident flux and the excitation cross section. The reduced escape depth  $l$  is given by  $1/l = 1/l_\alpha + 1/l_e$ , where  $l_\alpha$  ( $\sim 62 \text{ \AA}$ ) is the absorption length and  $l_e$  ( $\sim 25 \text{ \AA}$ ) is the electron escape depth.

To determine the depth dependence of the photothreshold, we need to solve Poisson's equation in the space charge region to find the valence band profile  $\Delta E(x)$ . The depth dependent photothreshold is defined as

$$E_T(x, N) = E_{\text{gap}}(N) + \chi - \Delta E(x), \quad (2)$$

where  $E_{\text{gap}}(N)$  is the band gap as a function of bulk doping  $N$ , and  $\chi$  is the electron affinity. The valence band profile  $\Delta E(x)$  is implicitly dependent on the doping concentration. For a lightly doped semiconductor the bands are flat, whereas the band curvature increases as the doping level increases. Figure 2 is an illustration of the band bending in a *p*-type semiconductor, which produces a depth dependent photothreshold. Notice that the energy necessary for a photoelectron to escape the top of the valence band and enter the vacuum decreases with bulk depth.

Another effect of increased doping concentration is the broadening of the impurity states near the band edge. For sufficiently high concentrations, the states merge with the continuous band resulting in a reduction of the band gap.<sup>8,9</sup> Since we are studying heavily doped silicon, it is necessary

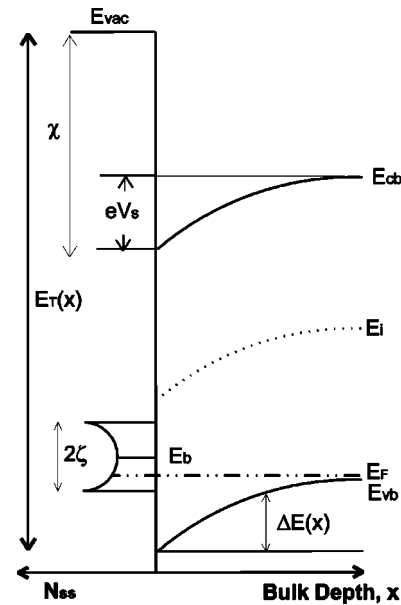


FIG. 2. Band bending diagram for *p*-type semiconductor with parabolic surface state distribution centered at charge neutrality level  $E_b$ . The band profile  $\Delta E(x)$  increases with bulk depth  $x$ . As a result, the photothreshold  $E_T(x)$  decreases as  $x$  increases.

to use the reduced band gap in determining the photothreshold as a function of doping concentration. From Wagner's published data,<sup>8</sup> the band gap for boron-doped silicon is reduced by approximately 50 and 160 meV for  $10^{18}$  and  $10^{20} \text{ cm}^{-3}$ , respectively.

The band profile  $\Delta E(x)$  can be expressed in terms of the local potential  $V(x)$

$$\Delta E(x) = E_{vb} - E_{vs} - eV(x), \quad (3)$$

where  $E_{vb}$  is the bulk valence band level,  $E_{vs}$  is the surface valence band level, and  $e$  is the positive electric charge. In the bulk, the potential  $V_b \equiv V(x \rightarrow \infty)$  is set to zero, while potential  $V_s$  is defined as  $V(x=0)$ . We use the subscripts  $s$  and  $b$  throughout to represent the surface and bulk, respectively. The magnitude of the band bending can be described by the potential difference between the surface and the bulk. For brevity and consistency with others,<sup>10-12</sup> we use the dimensionless quantities

$$v(x) = eV(x)/kT, \quad u(x) = (E_F - E_i(x))/kT$$

and

$$w_{p,q} = (E_p - E_q)/kT.$$

In this dimensionless form, the magnitude of the band bending is simply given by  $v_s$  since the bulk potential  $v_b$  is identically zero.

Poisson's equation in normalized units is expressed as

$$\frac{d^2 v}{dx^2} = \frac{-e}{\epsilon \epsilon_0 kT} [\rho_d + \rho_a + e(p - n)]. \quad (4)$$

Here the concentration of charge donor sites  $\rho_d$  and the concentration of charge acceptor sites  $\rho_a$  are given by

$$\rho_d = \frac{eN_d}{1 + 2 \exp[(E_F - E_d)/kT]},$$

$$\rho_a = \frac{-eN_a}{1 + 2 \exp[(E_a - E_F)/kT]}.$$

$E_d$  and  $E_a$  are the donor and acceptor impurity ionization energies, respectively. For boron in Si, the ionization energy  $E_a$  is approximately 46 meV. According to calculations done with Profile,<sup>13</sup> the impurity concentrations  $N_a$  and  $N_d$  are uniform in the region sampled by PEEM. Since we are interested in photoemission from semiconductors that are heavily to degenerately doped, the mobile charge carrier concentrations  $p$  and  $n$  are given by

$$p = 4\pi(2m_p^*kT/h^2)^{3/2} F_{1/2}(w_{v,i} - v - w_{F,ib}),$$

$$n = 4\pi(2m_n^*kT/h^2)^{3/2} F_{1/2}(v + w_{F,ib} - w_{c,i}),$$

where the subscript  $i$  refers to the intrinsic energy level and the Fermi–Dirac integral  $F_j(\eta)$  is

$$F_j(\eta) = \int_0^\infty \frac{e^j d\epsilon}{1 + \exp(\epsilon - \eta)}.$$

We follow the procedure outlined in Refs. 10–12 to solve Eq. (4). With this approach, it is necessary to determine the magnitude of the band bending  $v_s$  required to maintain charge neutrality given the distribution of surface states. The surface state charge density  $q_{ss}$  and the space charge density  $q_{sc}$  are computed, using  $v_s$  as a parameter, so that the condition

$$q_{ss} + q_{sc} = 0 \tag{5}$$

is met. Once the proper value of  $v_s$  necessary for neutrality is found, Poisson’s equation can be solved to give the potential as a function of bulk depth. Then, the valence band profile  $\Delta E(x)$  can be determined which in turn gives the depth dependence of the photothreshold  $E_T(x)$ .

The charge density in the surface states in the most general sense is given by

$$q_{ss} = e \int D_{sd}(E)[1 - f_d(E - E_F)]dE - e \int D_{sa}(E)f_d(E - E_F)dE, \tag{6}$$

where  $D_{sd}(E)$  is the distribution of donor-like surface states,  $D_{sa}(E)$  is the distribution of acceptor-like surface states, and  $f_d$  is the Fermi–Dirac function. The argument of the Fermi–Dirac function for a  $p$ -type semiconductor can be expressed in terms of  $v_s$  as

$$(E - E_F) = (E - E_{vs}) - v_s kT + kT \ln(N_a/N_v),$$

where  $N_v = 1.82 \times 10^{19} \text{ cm}^{-3}$  is the effective density of states in the bulk valence band.<sup>14</sup> For a  $n$ -type semiconductor the argument becomes

$$(E - E_F) = (E - E_{cs}) - v_s kT - kT \ln(N_d/N_c),$$

where  $N_c = 2.79 \times 10^{19} \text{ cm}^{-3}$  is the effective density of states in the bulk conduction band.<sup>14</sup> A linear interpolation of the

data published by Allen and Gobeli<sup>3</sup> is used to determine the position of the bulk Fermi level when the sample is degenerately doped.

We assume the density of states will be the same for all doping levels. We also assume that the total number of surface states cannot exceed the surface atomic density which for Si is approximately  $6.8 \times 10^{14} \text{ cm}^{-2}$ . Experimental evidence suggests that the density of surface states for oxide-covered Si(001) is U-shaped.<sup>15–17</sup> Thus, we consider the case of a parabolic distribution

$$D_{ss}(E) = C_1(E - E_b)^2 + C_2, \tag{7}$$

centered about the charge neutrality level  $E_b$  to calculate the surface state charge density  $q_{ss}$ . The charge neutrality level which acceptor-like states lie above and donor-like states lie below is located 0.36 eV above the surface valence band for Si.<sup>18</sup> The coefficient  $C_2 = 1.72 \times 10^{12} \text{ cm}^{-2} \text{ eV}^{-1}$  was determined from Angermann’s published data.<sup>17</sup> We vary the coefficient  $C_1$  to produce the desired magnitude of surface state density  $N_{ss}$ . The full width of the surface state distribution is defined as  $2\zeta$  as shown in Fig. 2.

In the case of discrete surface states, the surface states are positioned at a fixed energy level in the gap. We considered energy levels from 0.15 to 0.33 eV above the valence band maximum at the surface for the donor-like states associated with a surface oxide. The surface state charge density now becomes

$$q_{ss} = eN_{sd}(1 - f_d(E - E_F)) \tag{8}$$

where  $N_{sd}$  is the total number of surface donor states.

To determine the space charge density, we note that  $q_{sc}$  is given by

$$q_{sc} = (\epsilon\epsilon_0 kT/e)(dv/dx)_{\text{surface}}. \tag{9}$$

By integrating Eq. (4) and setting  $(dv/dx)_{\text{bulk}} = 0$ , the space charge density in terms of  $v_s$  is<sup>10</sup>

$$q_{sc} = \frac{\epsilon\epsilon_0 kT}{eL_D} \left[ \frac{N_d}{n_i} \ln \left( \frac{1 + 1/2 \exp(w_{d,i} - v_s - u_b)}{1 + 1/2 \exp(w_{d,i} - u_b)} \right) + \frac{N_a}{n_i} \ln \left( \frac{1 + 1/2 \exp(v_s + u_b - w_{a,i})}{1 + 1/2 \exp(u_b - w_{a,i})} \right) - \frac{2}{3F_{1/2}(w_{v,i})} [F_{3/2}(w_{v,i} - u_b) - F_{3/2}(w_{v,i} - v_s - u_b)] + \frac{2}{3F_{1/2}(w_{i,c})} [F_{3/2}(v_s + u_b - w_{c,i}) - F_{3/2}(u_b - w_{c,i})] \right]^{1/2}.$$

The Debye length  $L_D$  is defined as

$$L_D = \left( \frac{\epsilon\epsilon_0 kT}{2e^2 n_i} \right)^{1/2}$$

and  $n_i$  is the intrinsic carrier concentration given by

$$n_i = 4\pi(2m_n^*kT/h^2)^{3/2} F_{1/2}(w_{i,c}) \text{ (electrons)}$$

$$= 4\pi(2m_p^*kT/h^2)^{3/2} F_{1/2}(w_{v,i}) \text{ (holes)}.$$

TABLE I. Magnitude of band bending  $v_s$  for parabolic surface state distribution  $D_{ss}(E)$  with different surface donor concentrations  $N_{sd}$  when  $\zeta = 0.20$  eV.

$N_a$ ( $\text{cm}^{-3}$ )	$N_{sd}=10^{13}$ ( $\text{cm}^{-2}$ )	$N_{sd}=4 \times 10^{13}$ ( $\text{cm}^{-2}$ )	$N_{sd}=5 \times 10^{13}$ ( $\text{cm}^{-2}$ )	$N_{sd}=10^{14}$ ( $\text{cm}^{-2}$ )
$10^{17}$	5.06	6.42	6.63	7.28
$10^{18}$	5.11	7.11	7.41	8.29
$10^{19}$	4.57	7.98	8.39	9.54
$10^{20}$	2.98	9.21	9.87	11.5
$2 \times 10^{20}$	2.58	9.83	10.8	12.8

With  $q_{ss}$  and  $q_{sc}$  defined in terms of  $v_s$ , we can now use Eq. (5) to find the magnitude of band bending required for neutrality.

Since the quantities on the right side of Eq. (4) depend only on  $v_s$ , integrating twice gives the potential as a function of bulk depth. This solution along with Eq. (3) gives the valence band profile which in turn determines the depth dependent phototreshold for a given doping concentration.

To calculate the measured photoyield given the depth-dependent phototreshold, Eq. (1) must be integrated over the available photon energies found in the light source

$$Y_{\text{tot}} \propto \int g(h\nu)Y(h\nu)d h\nu, \quad (10)$$

where  $g(h\nu)$  represents the distribution of photon energies. As mentioned earlier, we use a Gaussian distribution with a full-width at half maximum of 0.13 eV to model the photon energy distribution from the Duke University FEL.<sup>5</sup>

In summary, the computation for B-doped silicon is done by first choosing a doping concentration  $N$  and surface state density  $N_{ss}$ . Equation (5) is then solved using either Eqs. (6) or (8) and Eq. (9) to find  $v_s$ . Then, Poisson's equation [Eq. (4)] is solved to generate the band bending profile  $\Delta E(x)$ . With  $\Delta E(x)$  known, Eq. (2) can be substituted into Eq. (1) to find the photoyield  $Y$  for a given photon energy, doping level, and surface donor concentration. Comparing the photoyield from Eq. (1) for each doping concentration of interest allows us to quantify the resulting contrast.

## RESULTS

We first consider the case of modeling the surface states with a parabolic function [Eq. (7)] centered about the charge neutrality level  $E_b$ . The photoyield was calculated at each experimental B doping level for a range of surface state densities  $N_{ss} = 10^{13}$  to  $6 \times 10^{14}$   $\text{cm}^{-2}$ . Several values of the distribution width,  $\zeta = 0.05, 0.10, 0.15,$  and  $0.20$  eV, were also evaluated. For each value of the density of surface states  $N_{ss}$ , the band bending  $v_s$  was calculated as a function of the bulk doping concentration  $N_a$ . Table I shows the range of  $v_s$  for four different surface donor concentrations when  $\zeta = 0.20$  eV. If the surface donor state density  $N_{sd} \geq 4 \times 10^{13}$   $\text{cm}^{-2}$  ( $N_{sd} = N_{ss}/2$ ), the magnitude of the band bending increases as the boron doping level increases. As a result, the absolute photoyield increases as the doping level  $N_a$  increases from  $10^{17}$  to  $2 \times 10^{20}$   $\text{cm}^{-3}$  as shown in the upper three curves in Fig. 3(a). For a density of surface donors

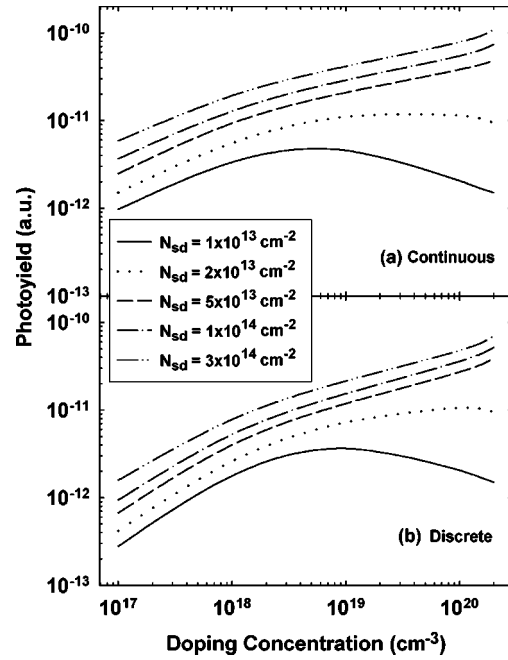


FIG. 3. Calculated effect of band bending on the photoyield for excitation at threshold,  $h\nu = E_\gamma(x=0)$ , as a function of  $p$ -type doping level. (a) Parabolic  $D_{ss}(E)$  with  $\zeta = 0.20$  eV. (b) Discrete  $D_{ss}(E)$  with surface donor level 0.16 eV above  $E_{vc}$ . In all cases, nonmonotonic behavior results if  $N_{sd}$  is not sufficiently large. Band gap reduction was not taken into account here.

$N_{sd} < 4 \times 10^{13}$   $\text{cm}^{-2}$ , the surface states become depleted of electrons for modest doping levels. Thus for higher doping levels, increased charge transfer is not possible. The magnitude of the band bending will decrease with increasing doping because  $v_s$  is now inversely proportional to  $N_a$ . As a result, the photoyield no longer increases monotonically with doping concentration. Figure 3(a) depicts the transition from nonmonotonic to monotonic behavior in the photoyield as a function of doping concentration  $N_a$ . For the case when the parabolic distribution width  $\zeta = 0.20$  eV, monotonic behavior of the photoyield occurs over the entire doping range of interest when the number of surface donors  $N_{sd}$  is increased from  $4 \times 10^{13}$  to  $3 \times 10^{14}$   $\text{cm}^{-2}$ .

The width of the continuous distribution  $\zeta$  was varied so that the end points of  $D_{ss}(E)$  corresponded roughly with the pinning positions reported by Himpsel<sup>19</sup> ( $E_F - E_{vs} = 0.19$  eV) and Mönch<sup>20</sup> ( $E_F - E_{vs} = 0.31$  eV). Specifically, when  $\zeta = 0.05$  eV the lower end point of  $D_{ss}(E)$  is at 0.36–0.05 eV and when  $\zeta = 0.20$  eV the lower end point of  $D_{ss}(E)$  is at 0.36–0.20 eV. Table II shows the effect of varying the surface state distribution width  $\zeta$  on the magnitude of band

TABLE II. Magnitude of band bending  $v_s$  for parabolic surface state distribution  $D_{ss}(E)$  with different widths  $\zeta$  when  $N_{sd} = 5 \times 10^{13}$   $\text{cm}^{-2}$ .

$N_a$ ( $\text{cm}^{-3}$ )	$\zeta = 0.05$ (eV)	$\zeta = 0.10$ (eV)	$\zeta = 0.15$ (eV)	$\zeta = 0.20$ (eV)
$10^{17}$	9.24	8.23	7.36	6.63
$10^{18}$	10.6	9.42	8.36	7.41
$10^{19}$	11.9	10.7	9.52	8.39
$10^{20}$	13.2	12.2	11.1	9.87
$2 \times 10^{20}$	13.3	12.8	11.9	10.8

TABLE III. Magnitude of band bending  $v_s$  for discrete distribution  $D_{ss}(E)$  when  $E_{sd} - E_{vs} = 0.16$  eV.

$N_a$ ( $\text{cm}^{-3}$ )	$N_{sd} = 10^{13}$ ( $\text{cm}^{-2}$ )	$N_{sd} = 4 \times 10^{13}$ ( $\text{cm}^{-2}$ )	$N_{sd} = 5 \times 10^{13}$ ( $\text{cm}^{-2}$ )	$N_{sd} = 10^{14}$ ( $\text{cm}^{-2}$ )
$10^{17}$	3.38	4.37	4.53	5.02
$10^{18}$	4.01	5.27	5.46	6.04
$10^{19}$	4.17	6.44	6.70	7.43
$10^{20}$	2.98	8.15	8.59	9.62
$2 \times 10^{20}$	2.58	9.11	9.80	11.1

bending  $v_s$  when  $N_{sd} = 5 \times 10^{13} \text{cm}^{-2}$ . As  $\zeta$  is increased from 0.05 to 0.20 eV, the magnitude of the band bending  $v_s$  decreases significantly. However, the difference between the magnitude of the band bending at  $N_a = 10^{17}$  and  $2 \times 10^{20} \text{cm}^{-3}$  is approximately constant at  $v_s = 4$  in each case. As a result, there is no noticeable change in the relative photoyield for the different doping levels. There is also no change in the doping-induced contrast as the width of the surface state distribution is varied at a constant surface state density  $N_{ss}$ .

The results for the parabolic distribution were compared with the results for discrete surface donor states. The configurations considered covered a range of densities from  $N_{sd} = 10^{13}$  to  $3 \times 10^{14} \text{cm}^{-2}$ , each for discrete energy levels situated 0.16, 0.21, 0.26, and 0.31 eV above the surface valence band. In Table III, we present the band bending values  $v_s$  for a discrete state at 0.16 eV above the valence band for the same surface donor concentrations  $N_{sd}$  listed in Table I for comparison. As found in the continuous case, the magnitude of band bending increases with doping concentration for  $N_{sd} > 3 \times 10^{13} \text{cm}^{-2}$ . As a result, the absolute photoyield increases with doping concentration as long as the surface state density is large enough to cause Fermi level pinning, as shown in Fig. 3(b). In addition, when the surface donor concentration  $N_{sd}$  is increased, the absolute photoyield for each doping level also increases. However, there is only a slight change in the relative photoyields and thus the contrast as  $N_{sd}$  increases. The photoyields shown in Fig. 3(b) were calculated for a discrete level 0.16 eV above the surface valence band.

Band bending values for the remaining discrete energy levels, 0.21, 0.26, 0.31 eV, are listed in Table IV. As the discrete level moves toward the neutrality level, the band bending and the absolute photoyield for each doping concentration increases. However, the relative band bending and thus the doping-induced contrast changes little.

TABLE IV. Magnitude of band bending  $v_s$  for various discrete energy levels when  $N_{sd} = 5 \times 10^{13} \text{cm}^{-2}$ .

$N_a (\text{cm}^{-3})$	$(E_{sd} - E_{vs}) = 0.21$ (eV)	$(E_{sd} - E_{vs}) = 0.26$ (eV)	$(E_{sd} - E_{vs}) = 0.31$ (eV)
$10^{17}$	5.90	7.33	8.82
$10^{18}$	6.98	8.55	10.1
$10^{19}$	8.31	9.93	11.5
$10^{20}$	10.1	11.6	13.0
$2 \times 10^{20}$	11.2	12.4	13.2

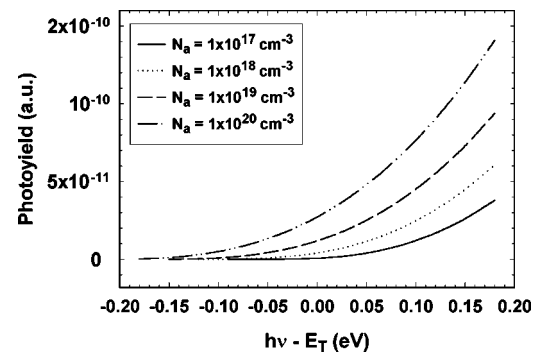


FIG. 4. Calculated effect of band bending on the photoyield as photon energy is varied across the nominal photothreshold  $E_T(x=0)$ . The case shown is for a discrete surface state at 0.16 eV above the surface valence band. There is a strong variation in photothreshold energy as a function of the doping level.

Up to this point, all the calculations have been for photoemission at the nominal threshold [i.e.,  $h\nu = E_T(x=0)$ ]. In addition, the effect of varying the photon energy on the calculated photoyield was also examined. In Fig. 4, the effect of the band bending on the calculated photoyield, as the photon energy is varied across the nominal threshold value for various doping concentrations, is shown. A discrete surface state energy level at  $E_{sd} - E_{vs} = 0.16$  eV with  $N_{sd} = 5 \times 10^{13} \text{cm}^{-2}$  was used to generate the curves. Obviously, there is nonzero photoemission below the nominal photothreshold [ $h\nu = E_T(x=0)$ ], which is caused by the band bending. As the boron doping concentration increases from  $10^{17}$  to  $10^{20} \text{cm}^{-3}$ , the amount of subthreshold photoyield increases. For  $N_a = 10^{17} \text{cm}^{-3}$ , photoemission extends about 0.1 eV below threshold consistent with band bending of approximately 0.1 eV ( $v_s = 4.53$ ). As the doping level increases to  $10^{20} \text{cm}^{-3}$ , subthreshold photoemission extends approximately 0.2 eV below the nominal threshold, again consistent with band bending of 0.2 eV ( $v_s = 8.59$ ). As a result, the model predicts that doping-induced contrast in the photoyield will change for incident photon energies below the nominal threshold value. This change will be manifested as the disappearance of signal from regions of lower doping with decreasing photon energy. The effect of explicitly including band gap reduction  $\Delta E_{\text{gap}}$  in the calculation of the photoyield is shown in Fig. 5. As expected, band gap reduction causes further depression of the photothreshold. For  $\Delta E_{\text{gap}} = 40$  meV (the value we used to fit data in Ref. 1), photoemission is extended approximately an additional 40 meV below the  $\Delta E_{\text{gap}} = 0$  meV threshold. Using a band gap reduction value ( $\Delta E_{\text{gap}} = 160$  meV) similar to values reported for heavily B-doped Si from photoluminescence excitation measurements,<sup>8</sup> photoemission is extended even further to approximately 300 meV below the nominal photothreshold.

Experimentally, the dependence of doping-induced contrast on photon energy was probed by imaging a device with adjacent lines of boron doping density  $N_a = 10^{18}$  and  $10^{20} \text{cm}^{-3}$  while tuning the incident photon energy from 4.5 to 5.2 eV. In Fig. 6, we show the results of imaging with photon energies  $h\nu = 4.8$  and 5.2 eV for comparison. The absolute image intensity in Fig. 6(a) was increased to levels comparable to Fig. 6(b), for visualization. At the initial photon en-

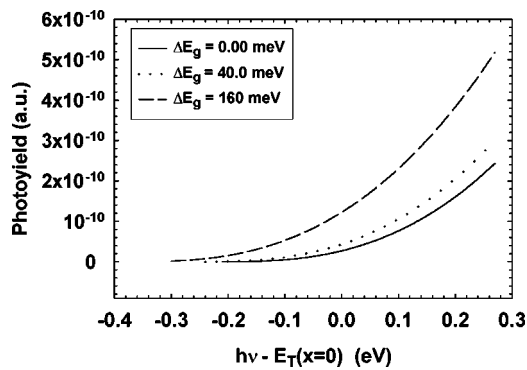


FIG. 5. Calculated effect of band gap reduction on the photoyield when  $N_a = 10^{20} \text{ cm}^{-3}$ . As the band gap is reduced, photoemission is extended further beyond the nominal photothreshold. The  $\Delta E_{\text{gap}} = 40 \text{ meV}$  curve produces a good fit to our data (see Ref. 1).  $\Delta E_{\text{gap}} = 160 \text{ meV}$ , taken from Fig. 11 in Ref. 8, is shown for comparison.

ergy  $h\nu = 4.5 \text{ eV}$ , only the  $N_a = 10^{20} \text{ cm}^{-3}$  B-doped stripe is observable. At approximately  $h\nu = 4.9 \text{ eV}$ , the articulated  $N_a = 10^{18} \text{ cm}^{-3}$  B-doped line also becomes visible. As the photon energy is increased to  $5.2 \text{ eV}$ , the intensity from both doping levels increases. The image clearly shows the persistence of photoyield from the higher doped line to lower values of the photon energy than for the lower doped line.

## DISCUSSION

All of the models considered for the surface state distribution gave consistent results for doping-induced contrast. This is in general agreement with what Allen and Gobeli reported.<sup>3</sup> Fitting the calculated photoyield as function of boron concentration to a power law, we find an exponent of 0.17 which corresponds to a gain of approximately 1.5 in intensity per decade of doping level. This is in rough agreement with a measured intensity gain of approximately 2 per decade of doping concentration. However, a minimum number of surface states is necessary to generate the observed doping-induced contrast. If the number of surface donor states  $N_{\text{sd}}$  is less than  $4 \times 10^{13} \text{ cm}^{-2}$ , the band bending does not increase monotonically with boron implant concentration. This nonmonotonic behavior comes about when all

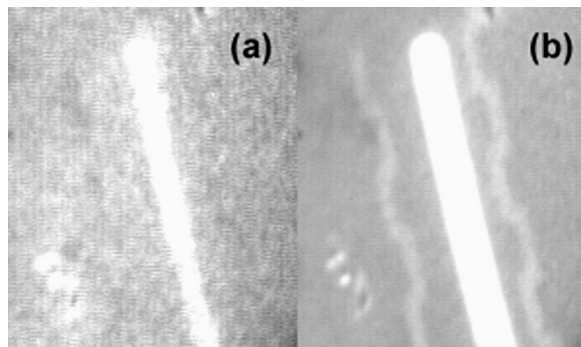


FIG. 6. FEL-PEEM image illustrating effect of incident photon energy on doping-induced contrast. (a) At  $h\nu = 4.8 \text{ eV}$ , only the  $10^{20}$  B-doped stripe is observable. (b) At  $h\nu = 5.2 \text{ eV}$ , both  $10^{18}$  and  $10^{20} \text{ cm}^{-3}$  B-doped lines are observable. The field of view is  $\approx 30 \mu\text{m}$  for both images. The image intensity in (a) has been enhanced roughly  $2\times$  for comparison with (b).

available surface states are charged. Thus, the maximum surface charge density for a given surface state density will be achieved. Beyond this point, the amount of band bending necessary to generate an equal and opposite amount of charge in the material decreases as the doping level  $N_a$  is increased, and as a result the photoyield begins to drop. Thus, the model predicts that contrast between different  $p$ -type regions can be reversed for a sufficiently low density of surface states.

While the contrast is largely unaffected by changes in the surface state distribution, the absolute photoyield is affected. For a fixed surface state distribution, either parabolic or discrete, the photoyield increases as the areal surface state density increases. The photoyield will also increase as the position of the discrete surface states above the surface valence band is increased. In addition, narrowing the width of the continuous distribution  $\zeta$ , which is the equivalent to increasing the energy density of the surface states, results in a higher absolute photoyield.

However, the curvature of the valence band causes the photothreshold to decrease with increasing doping, suggesting that varying the incident photon energy will affect the contrast between different levels of  $p$ -type doping. Tuning the incident photon energy allows us to experimentally test how doping-induced contrast is affected. Experimentally, we indeed observe a decrease in the photothreshold as the doping level increases. At the same time, the measured photoyield decreases as the photon energy is lowered toward the threshold value. Therefore, discrimination between two different boron doped levels can be removed by imaging below the higher threshold of the two. Conversely, increasing the photon energy above threshold will increase the photoyield, but the contrast is limited by the dynamic range of the imaging detector. Therefore, the optimum doping-induced contrast is achieved by imaging with a photon energy slightly above the highest threshold of interest to generate a sufficient signal-to-noise ratio for imaging the lowest doping level of interest.

We briefly discuss evaluation of the model parameters necessary to describe the image data. As can be seen in Fig. 4 (and also Fig. 2 of Ref. 1), the variation of photoyield with  $h\nu$  can be described by an upward energy dependent curvature and a low energy cutoff. Fits to the experimental data tend to emphasize the overall energy dependence where the photoyield is higher. Since the low energy cutoff is a function of doping, both the nominal photothreshold  $E_T(0)$  and the band gap reduction  $\Delta E_{\text{gap}}(n)$  need to be adjusted. For the data of Ref. 1,  $E_T(0)$  is set and then  $\Delta E_{\text{gap}}(n)$  was adjusted at each doping level to get the proper fit of the photoyield versus photon energy dependence. We found a band gap reduction value of  $40 \text{ meV}$  at  $3 \times 10^{19} \text{ cm}^{-3}$ , substantially less than the photoluminescence excitation value ( $130 \text{ meV}$  at  $3 \times 10^{19} \text{ cm}^{-3}$ ) reported by Wagner,<sup>8</sup> produces a reasonable fit to the observed curvature of the intensity versus photon energy using  $E_T(x=0) = 4.9 \text{ eV}$ .

Yet, as noted above, we observe contrast at  $h\nu = 4.5 \text{ eV}$  between the  $N_a = 10^{20} \text{ cm}^{-3}$  boron-doped region and the lightly  $n$ -doped substrate. Photoemission at  $0.4 \text{ eV}$  below the nominal threshold would require band gap reduction on the

order of 200 meV. This is consistent with values in Ref. 8, but the fits to our data using this value do not fit the curvature of the data at higher energy nearly as well.

The discrepancy in fitting the data may arise in part due to the assumption made in determining the space charge density that the impurities are noninteracting. However, this is only appropriate for lightly doped semiconductors. As mentioned earlier, the impurity states broaden as the implant concentration increases until there is a reduction in the band gap. Yet, band gap reduction is explicitly taken into account in Eq. (2). This may explain why the gap reduction values that we reported previously<sup>1</sup> are lower than that reported by Wagner.<sup>8</sup> Possibly, the error in the space charge calculation is compensated for by decreasing the amount of band gap reduction necessary to fit the data. The reader is referred to Ref. 10 for a more complete discussion on the validity of the space charge density calculation.

In addition to band gap narrowing, we consider the possible contribution of surface state emission to photoemission extending far below the nominal phototreshold. While photoemission from occupied surface states can contribute to the total photoyield, the number of occupied surface states decreases with increasing  $p$  doping because as band bending increases the position of the surface Fermi level moves away from the charge neutrality level. Hence, the surface state contribution to the total photoyield decreases as the doping concentration increases. Experimentally, we observe photoemission from the higher doped regions at lower photon energies as the incident photon energy is decreased. Thus, photoemission from occupied surface states cannot explain the persistent intensity from the  $10^{20} \text{ cm}^{-3}$   $p$  stripe in the low energy FEL-PEEM images.

## CONCLUSIONS

In modeling doping-induced contrast from a native oxide covered  $pn$  array fabricated on a Si(001) surface, we have considered both continuous (parabolic) and discrete surface state distributions. In either case, we find that a surface donor concentration  $N_{sd}$  of approximately  $5 \times 10^{13} \text{ cm}^{-2}$  is necessary for the calculated PEEM intensities to increase monotonically with boron doping concentration  $N_a$ . This results in contrast between heavily doped implant regions. If the density of surface states is greater than the minimum necessary for doping-induced contrast to occur, then varying the position and uniformity of the surface states will not affect the doping-induced contrast. However, if the number of surface donors is too small, the calculated intensity ratios will not increase as the boron doping level is increased. Thus, the model sets a lower bound on the density of surface states necessary to describe the measured doping-induced contrast in Si(001). In addition, the valence band profile generated by

this model predicts that doping-induced contrast can be affected by varying the incident photon energy. Experimentally, we find that the contrast between heavily doped boron regions is affected by the excitation energy. The visibility of boron implanted regions can be removed by imaging with a photon energy less than its effective phototreshold. We find that a model which includes surface state effects and band gap reduction explains most of the variation we observe with photon energy, although the doping dependent low energy cutoff is difficult to model. Finally, we mention that the model presented is general enough to model and predict doping-induced contrast in PEEM of other semiconductors.

## ACKNOWLEDGEMENTS

This work would not be possible without the collaboration of the Duke University Free Electron Laser Laboratory and Professor R. J. Nemanich (NCSU). The authors would also like to thank W.-C. Yang and the FEL staff for their generous assistance. They also acknowledge A. Fernandez and S. Mogren for their work in fabricating the samples. This work was supported by the Laboratory for Physical Sciences.

- <sup>1</sup>V. W. Ballarotto, K. Siegrist, R. J. Phaneuf, and E. D. Williams, *Appl. Phys. Lett.* **78**, 3547 (2001).
- <sup>2</sup>V. W. Ballarotto, K. Siegrist, R. J. Phaneuf, and E. D. Williams, *Surf. Sci.* **461**, L570 (2000).
- <sup>3</sup>F. G. Allen and G. W. Gobeli, *Phys. Rev.* **127**, 150 (1962).
- <sup>4</sup>M. Giesen, R. J. Phaneuf, E. D. Williams, T. L. Einstein, and H. Ibach, *Appl. Phys. A: Mater. Sci. Process.* **64**, 423 (1997).
- <sup>5</sup>H. Ade *et al.*, *Surf. Rev. Lett.* **5**, 1257 (1998).
- <sup>6</sup>M. L. Hildner, R. J. Phaneuf, and E. D. Williams, *Appl. Phys. Lett.* **72**, 3314 (1999).
- <sup>7</sup>E. O. Kane, *Phys. Rev.* **127**, 131 (1962).
- <sup>8</sup>J. Wagner, *Phys. Rev. B* **29**, 2002 (1984).
- <sup>9</sup>S. T. Pantelides, A. Selloni, and R. Car, *Solid-State Electron.* **28**, 17 (1985).
- <sup>10</sup>R. Seiwatz and M. Green, *J. Appl. Phys.* **29**, 1034 (1958).
- <sup>11</sup>H. Lüth, *Surfaces and Interfaces of Solid Materials*, 3rd ed. (Springer, Berlin, 1995), Chap. 7.
- <sup>12</sup>W. Mönch, *Semiconducting Surfaces and Interfaces*, 2nd ed. (Springer, Berlin, 1995), p. 17 and Chap. 2.
- <sup>13</sup>Computer code PROFILE version 3.20, distributed by Implant Sciences Corporation. Calculates one-dimensional implant profiles with pre- and post-annealing simulations.
- <sup>14</sup>Landolt-Börnstein, in *Numerical Data and Functional Relationships in Science and Technology*, edited by O. Madelung (Springer, Berlin, 1982), Vol. III/17.
- <sup>15</sup>M. H. White and J. R. Cricchi, *IEEE Trans. Electron Devices* **19**, 1280 (1972).
- <sup>16</sup>S. Koyanagi, T. Hashizime, and H. Hasegawa, *Jpn. J. Appl. Phys., Part 1* **35**, 946 (1996).
- <sup>17</sup>H. Angermann, W. Henrion, M. Rebien, D. Fischer, J.-T. Zettler, and A. Röseler, *Thin Solid Films* **313–314**, 552 (1998).
- <sup>18</sup>J. Tersoff, *Phys. Rev. Lett.* **52**, 465 (1984).
- <sup>19</sup>F. J. Himpsel, B. S. Meyerson, F. R. McFeely, J. F. Morar, A. Taleb-Ibrahimi, and J. A. Yarmoff, *Photoemission and Absorption Spectroscopy of Solids with Synchrotron Radiation* (North Holland, Amsterdam, 1990), p. 211.
- <sup>20</sup>W. Mönch, P. Koke, and S. Krueger, *J. Vac. Sci. Technol.* **19**, 313 (1981).